CREEP STRENGTH OF HIGH CR FERRITIC STEELS DESIGNED USING NEURAL NETWORKS AND PHASE STABILITY CALCULATIONS

F. Masuyama* and H.K.D.H. Bhadeshia**

*Kyushu Institute of Technology
Graduate School of Engineering
1-1, Sensui-cho, Tobata, Kitakyushu 804-8550, Japan

**University of Cambridge
Department of Materials Science and Metallurgy
Pembroke Street, Cambridge CB2 3QZ, U.K.

Abstract

The highest creep rupture strength of recent 9-12%Cr steels which have seen practical applications is about 130 MPa at 600°C and 100,000 h. While the 630°C goal may be realized, much more work is needed to achieve steam temperatures up to 650°C. Conventional alloy development techniques can be slow and it is possible that mathematical models can define the most economical path forward, perhaps leading to novel ideas. A combination of mechanical property models based on neural networks, and phase stability calculations relying on thermodynamics, has been used to propose new alloys, and the predictions from this work were published some time ago. In the present work we present results showing how the proposed alloys have performed in practice, considering long term creep data and microstructural observations. Comparisons are also made with existing enhanced ferritic steels such as Grade 92 and other advanced 9-12%Cr steels recently reported.

Introduction

Development of heat-resistant steel for power boilers and turbines has been ongoing for about five decades. This has led to an increase in the thermal efficiency of power plants whenever innovative steels have been commercially implemented. Through this effort, the steam conditions, temperature and pressure of power plants have recently been raised to about 600°C and 35 MPa using ferritic steels for improved efficiency in response to environmental protection and energy conservation requirements (1). Further enhancements in the creep resistance of 9-12%Cr steels used for boiler header/piping and steam turbine rotor applications are vital in order to achieve steam temperatures in excess of 630°C. Ferritic steels developed to date have

maximum creep rupture strengths of approximately 130 MPa at 600°C and 65 MPa at 650°C for 100,000 hours. However there is strong demand for the development of ferritic steels having a strength of 100 MPa at 650°C for future advanced plants, including a 700°C class (2). According to conventional alloy development techniques, creep strength can be improved by optimizing chemistry and heat treatment based on experience and test results of creep data obtained after long-term creep tests for several years or more. This can be a very slow way forward. It is possible that we are now at the limits of what can be achieved with ferritic steels. Given this situation, it is possible that mathematical models can provide the most economical path, with a different approach to alloy development (3).

A combination of mechanical property models based on neural networks, together with phase stability calculations relying on thermodynamics, has been used to propose new ferritic steels, and the predictions from this work were published some time ago (4). The published work predicted excellent stress rupture strength, double or greater than that of the strongest steel developed to date. However, such predictions remain to be tested experimentally. Accordingly, two of the proposed steels and one standard steel were melted to be manufactured as wrought materials, and their creep rupture properties and microstructures were investigated for comparison with the predicted results. Based on this comparison, differences between the predictions and experimental results are discussed.

Analysis and Predicted Properties of the Proposed Steels (4)

Neural networks now comprise a general method of non-linear regression analysis in which a mathematical relationship is established between each of the independent input variables, x_j and one or several dependent output variables, y. In linear regression analysis, the sum of all products x_j multiplied by a weight w_j and a constant θ then gives an estimate of the $y = \sum_j w_j x_j + \theta$.

Neural networks are in general non-linear and the non-linearity is achieved by taking a hyperbolic tangent of the right hand side of this equation, and then applying a linear transfer into y. In fact, many hyperbolic tangents and corresponding weights can be added to make the function as complex as is necessary. The relationship is generated by presenting a network with a database consisting of a set of input conditions for which the value is known. The network then learns a relationship between the input conditions and corresponding values for the output in a procedure that is known as training the network. Once the network is trained, output prediction (creep rupture strength in the present study) for any given inputs such as chemical composition and heat treatment condition is very rapid. However, there are no physical models for the output parameters or creep rupture strength. An example of the neural network structure is shown in Figure 1. In the present study the network consisted of 37 input nodes (one for each variable), a number of hidden nodes and an output node representing the creep rupture strength. The hidden nodes are where the mathematical operations described below are carried out. More hidden nodes represent a more complex model. The network was trained using 1033 examples randomly chosen from a total of 2066 available, which are combinations of creep rupture strength and 30
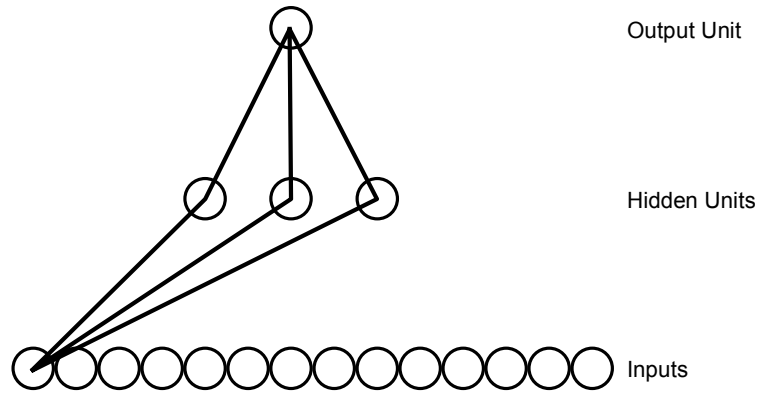
Fig.1　A typical three-layer network in the analysis

original inputs including the time to rupture, chemical composition, and heat treatment in the database compiled from 27 published reports, with the remaining 1033 examples being used as new experiments to test the trained network.

Linear functions of the inputs x_j are operated on by the hyperbolic tangent transfer function:

$$h_i = \tanh\left(\sum_j w_{ij}^{(1)} + \theta_i^{(1)} \right) \tag{1}$$

so that each input contributes to every hidden unit. The bias is designated θ_i and is analogous to the constant that appears in linear regression. The strength of the transfer function is in each case determined by the weight w_{ij}. The transfer to the output y is linear:

$$y = \sum_i w_{ij}^{(2)} + \theta^{(2)} \tag{2}$$

The specification of the network structure, together with the set of weights is a complete description of the formula relating the inputs to the output.

To explore the network, a study was made on the behavior of the model for two classic steels: 2.25Cr-1Mo (Grade 22 steel bainitic) and 10CrMoW (similar in composition to Grade 92 steel martensitic, but containing 0.86%Cu and higher Cr content of 10.61% - all concentrations in wt%). The resulting calculated curves of creep rupture strength as a function of time corresponded well to the actual strength for both steels, and trend curves for the effects of alloying elements and heat treatment conditions on the creep rupture strength were also developed and demonstrated.

Based on the findings by neural network analysis, innovative steels were proposed with creep rupture strengths. Table 1 shows the compositions emerging from the design, as well as the analyzed chemical composition of the manufactured steels. Table 2 shows the designed heat

Table 1 Input parameters on chemical composition and analysis of test steels

(mass%)

Steels		C	Si	Mn	P	S	Cr	Mo	W	Ni	Cu	V	Nb	N	Al	B	Co	Ta	O	Re
A	Input	0.12	0.00	0.48	0.0016	0.001	9.00	0.75	3.00	0.00	0.00	0.21	0.01	0.064	0.000	0.0080	1.25	0.0003	0.01	0.0003
	Analysis	0.11	<0.01	0.49	0.003	0.001	9.04	0.74	2.99	0.01	<0.01	0.20	0.011	0.064	0.004	0.0070	1.25	<0.0001	0.003	0.0003
B	Input	0.13	0.00	0.50	0.0016	0.001	8.70	0.30	3.00	0.00	0.00	0.21	0.01	0.064	0.000	0.0080	0.00	0.0003	0.01	0.0003
	Analysis	0.13	<0.01	0.50	0.002	0.001	8.75	0.30	2.99	<0.01	<0.01	0.20	0.011	0.068	0.003	0.0078	0.01	<0.0001	0.002	0.0006
N	Input	0.12	0.05	0.64	0.016	0.001	10.61	0.44	1.87	0.32	0.86	0.21	0.01	0.064	0.022	0.0022	0.02	0.0003	0.01	0.0003
	Analysis	0.12	0.04	0.64	0.018	0.001	10.65	0.43	1.87	0.32	0.85	0.20	0.011	0.072	0.021	0.0024	0.01	< 0.0001	0.003	0.0006

Table 2 Input parameters on heat treatment conditions applied to test steels

Steels	Normalizing			Tempering			Annealing		
	Temp. (℃)	Duration (h)	Cooling Rate	Temp. (℃)	Duration (h)	Cooling Rate	Temp. (℃)	Duration (h)	Cooling Rate
A	1200	2	AC	800	4	AC	740	4	AC
B	1180	2	AC	800	4	AC	740	4	AC
N	1065	2	AC	770	4	AC	740	4	AC

treatment parameters which were actually applied to the test steels. Steels A and B are proposed steels which are modified from the above-mentioned model or standard steel, 10CrMoW (steel N in Table 1). The first attempt led to the design of steel A, but its long term strength at 650°C barely failed to meet the 100 MPa requirement. Changes were thus made to improve both the mean long term strength and the certainty of prediction, reducing the cobalt, chromium and molybdenum concentrations, with the resulting material designated as steel B. The newly designed steels A and B do not contain any silicon, aluminum, nickel or copper, which are well known to cause deterioration in creep rupture strength. The boron concentration is reduced primarily to reduce the uncertainty of the predictions. There is also an increase in the normalizing temperature, as well as reductions in the manganese and chromium concentrations together with an increase in the level of tungsten. Consequently, the predicted 100,000 h creep rupture strength of each steels were 240-340 MPa, 230-310 MPa and 110-130 MPa at 600°C for steels A, B and N (10CrMoW) respectively, and 80-200 MPa, 130-180 MPa and 40-70 MPa at 650°C for steels A, B and N respectively. The predicted creep rupture strengths of Steels A and B are highly distinguished. The strength of steel N approaches the level of Grade 92, which is the highest among all steels commercially developed to date. If the mean values of the predicted 100,000 h creep rupture strengths of steels A and B are compared to steel N, steels A and B would exhibit approximately 2.5 times the strength of steel N at 600°C and 650°C.

In conjunction with the neural network calculation, phase diagram calculations and kinetic predictions through the calculation of precipitation reactions on the basis of thermodynamic data

and kinetic theory were also carried out. As a result of those calculations, it is predicted that the equilibrium fractions are $M_{23}C_6$ and Laves phase in each of the steels, and that the Laves phase only occurs in steel N (10CrMoW) at the very late stage of annealing at 650°C. Steels A and B were not found to exhibit Laves phase precipitation, at least at 10^6 h at 600°C or 650°C.

Test Materials and Experimental Procedures

The above-mentioned steels A and B designed using neural networks and phase stability calculations, proposed as new strong ferritic steels for power plant applications, were melted in a vacuum furnace as well as a standard material consisting of steel N (10CrMoW). Melted ingots weighing 20 kgf were forged to bars with sectional dimensions of 20 mm by 40 mm. Chemical compositions analyzed in comparison with target values, i.e., the input or predicted design parameters and heat treatment conditions of the test steels, are shown in Tables 1 and 2, respectively. Hardness measurement of the test steels (steels A, B and N) indicated 214, 216 and 225 respectively in terms of Vicker's hardness. Tensile strength at room temperature of the test steels showed a trend similar to that of hardness, indicating 659 MPa, 675 MPa and 715 MPa for steels A, B and N respectively, but the elevated temperature tensile strength of steels A and B turned out to be greater than for steel N at the temperature of 700°C. Values were 229 MPa and 233 MPa for steels A and B respectively, against 217 MPa for steel N. Creep tests were carried out at the temperatures of 600°C, 650°C and 700°C for a maximum duration of 23,500 h. Creep strain measurement and microstructural studies were also performed for comparative study of the creep deformation behavior among the test steels, as well as comparison of the precipitation properties with the predicted results.

Creep Properties of the Designed Steels

Figure 2 shows rupture stress versus time to rupture diagrams at the temperatures of 600°C, 650°C and 700°C for steels A, B and N. In the graph, the creep rupture data for Grade 92 (5) are also plotted with the average lines obtained by parametric analysis for the purpose of comparison. Steel N is slightly weaker than Grade 92 at 600°C, and the difference in strength between the two becomes greater at 650°C and 700°C with increased temperature. The strengths of steels A and B are nearly the same and lie on the upper bound or on a slightly stronger level than the Grade 92 data band at the temperatures of 600°C and 650°C, but at 700°C steel B shifts to the average line of Grade 92, and steel A shifts to the lower bound of the data band. Figure 3 demonstrates the Larson-Miller plot of the data for the three test steels. A parameter constant of 34.1 was selected as best fitting the average strength of Grade 92, but this value does not provide the best fit to the test steels in the entire parameter range. From the Larson-Miller master curve, the 100,000 h creep rupture strengths of the test steels were predicted as 129 MPa, 133 MPa and 108 MPa at 600°C, and 74 MPa, 76 MPa and 56 MPa at 650°C for steels A, B and N, respectively. Meanwhile, the strength of Grade 92 was predicted as 122 MPa at 600°C and 64 MPa at 650°C. Figure 4 visually illustrates the comparison of creep rupture strength estimated by neural network analysis and measured with respect to the actually melted test specimens, as well

as the measured tensile strength in the graph appearing in previously published literature (4). The measured creep rupture strength of steel N is generally observed in the band close to the predicted line with statistical deviation, while the strengths of steels A and B lie on the upper bound or slightly toward high stress at 600°C, but slightly stronger than the predicted line for Steel N at 650°C. The prediction of rupture stress versus time to rupture for steel N corresponds
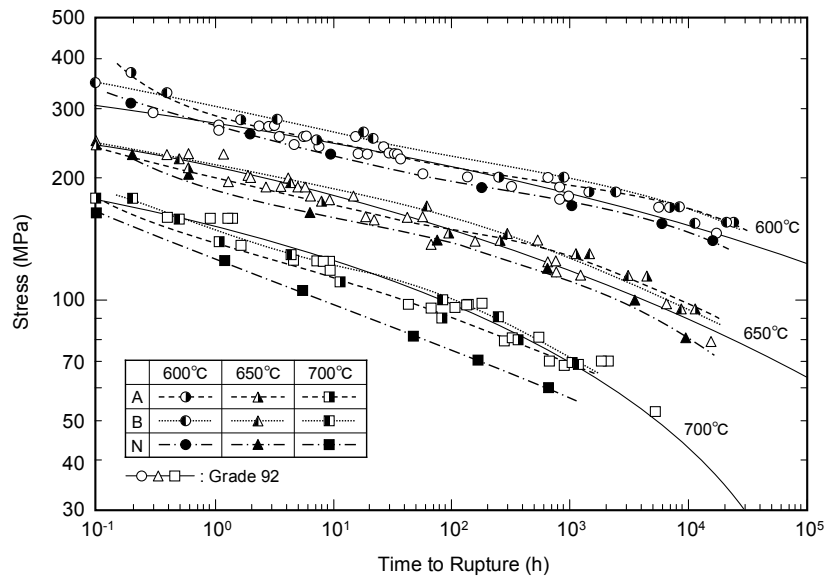
Fig.2 Stress vs. time to rupture diagrams at 600℃, 650℃ and 700℃ for test steels

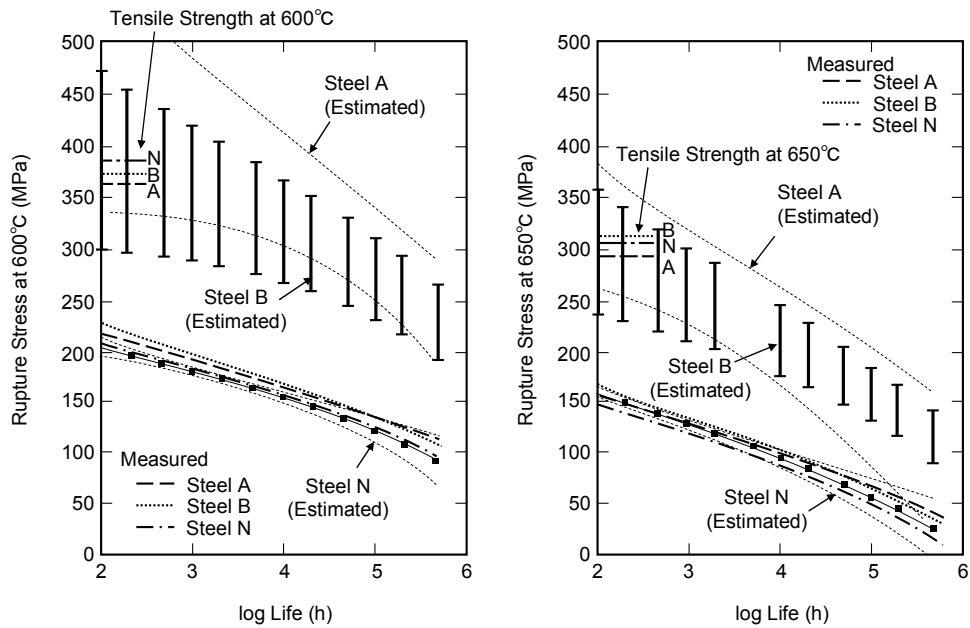Fig.3 Larson-Miller parameter plots of creep rupture strength of test steels

Fig.4 Comparison of creep rupture strength between predictions and measured results

very well to the measured results at 600°C, and shifts slightly in a parallel manner towards the weaker direction at 650°C.

Figure 5 shows the creep deformation behaviors of the test steels at 650°C. The primary creep rates of the test steels start at the same value and decrease along nearly the same line despite the different test stress conditions, and then start tertiary creep at different minimum creep rates

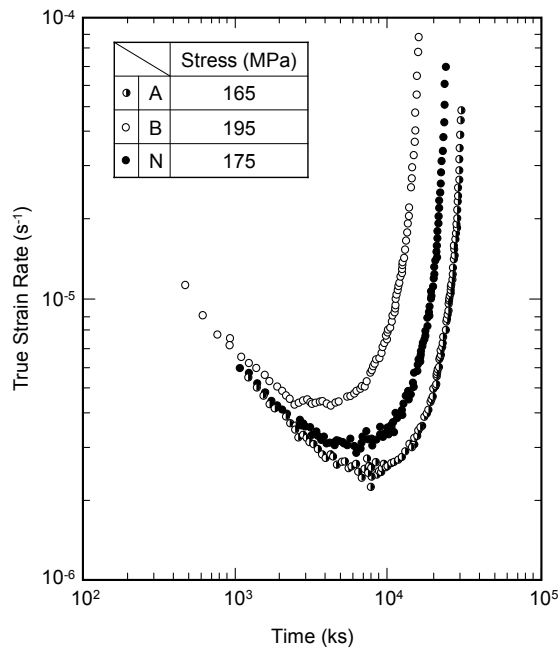|		Stress (MPa)
◔	A	165
○	B	195
●	N	175

Fig.5 Creep deformation behaviors of test steels at 650°C

depending on the stress and the material. However, the tertiary creep curves of the three steels behave according to a similar trend, suggesting that the same mechanisms govern the creep. Figure 6 shows the average creep rate versus stress relationship for the test steels. It is confirmed that the average creep rate is proportional to the minimum creep rate, with a coefficient of approximately 0.98 x 10^1 across the entire range of stress (6). Norton's law therefore applies to the relationship between average creep rate and stress. At the temperatures of 600°C and 650°C, very high stress exponent values such as 16 and 25 are seen (25 in the case of steel A only, at the lower stress range below the stress which lead 16). This means that the steels are highly strengthened by precipitations promoting a large amount of internal stress. At the temperature of 700°C, the stress exponent is in the range of 8 to 11 with moderate strengthening by precipitation.
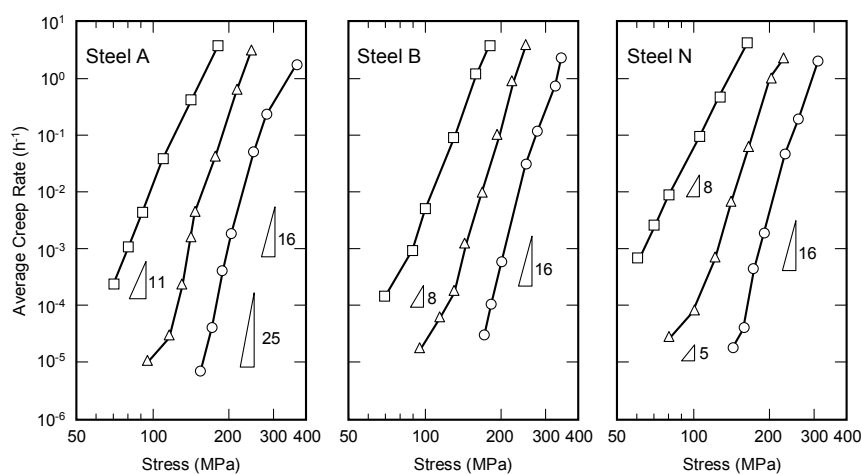

Fig.6 Creep rate vs. stress relationship for test steels

Microstructures of the Designed Steels

Figure 7 shows optical micrographs of the as-manufactured or creep ruptured test steels. Steels A and B exhibit courser prior austenite grain size than steel N, and very tight martensite lath structures are observed in each of the steels before and after the creep test. The crept specimens include recovered lath structures at certain locations in the grains, but it is hard to distinguish the recovered lath in the complicated fine structures. Figure 8 shows highly magnified transmission electron micrographs of the creep ruptured test steels. The martensite lath grain exhibited reduced dislocation density, with recovery to subgrain structures. Precipitations are observed along the grain boundaries and the interior of the recovered subgrain. Figures 9 and 10 show FE-SEM graphs of as-manufactured and creep ruptured test steels respectively. The as-manufactured specimens were observed using secondary electron imaging (SEI) and back scattered electron imaging (BEI), but the creep ruptured specimens were viewed only by BEI. The SEI graph displays all of the precipitation as white points, while the BEI graph displays the precipitates containing heavy elements such as molybdenum and tungsten as bright points, meaning that the bright points correspond to the Laves phase in the present study. The SEM graph of the as-manufactured specimen in Figure 9 shows numerous fine precipitates along the grain boundaries.

On the other hand, in the case of the BEI graph, only steel A shows a number of bright points corresponding to the Laves phase, while steels B and N show no bright spots. The BEI graphs of the gauge portion and grip portion of the creep ruptured specimens show numerous Laves phase precipitation along the prior austenite grain boundaries and packet/block boundaries. The fact that there is no notable difference between the gauge and grip portions means that the stress does not influence the Laves phase precipitation. The observation of FE-SEM structures and other element analysis such as EPMA clarified that all the test steels formed precipitates of $M_{23}C_6$ and
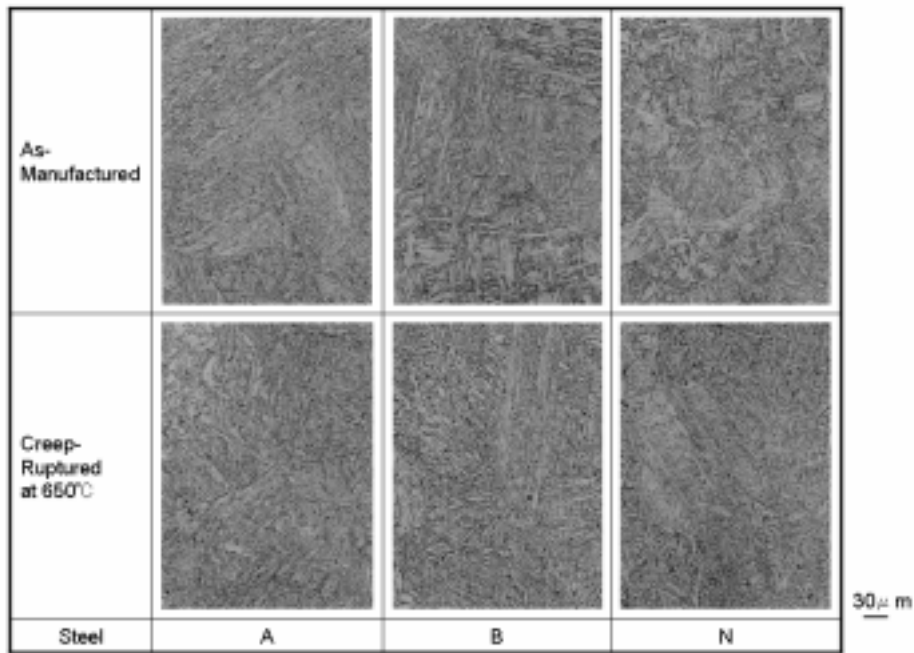

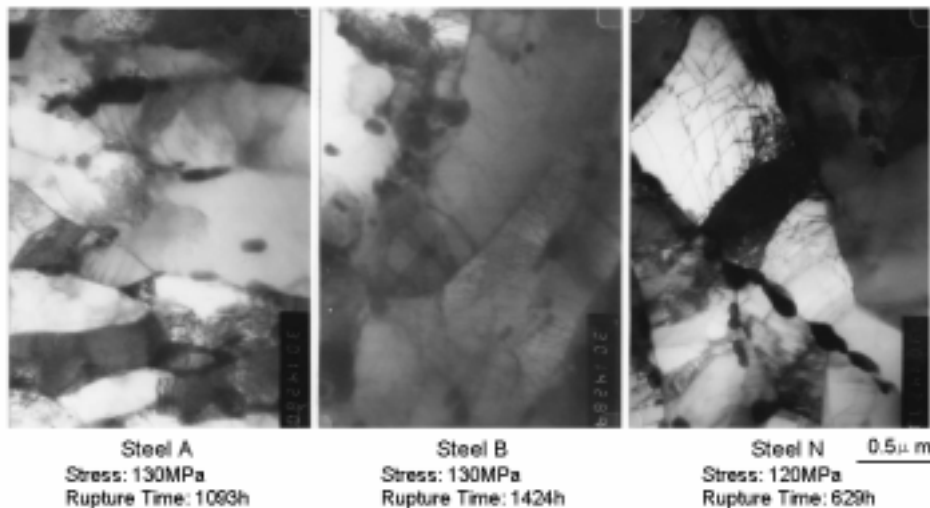Fig.7 Microstructures of tested steels as manufactured or creep-ruptured

Steel A
Stress: 130MPa
Rupture Time: 1093h

Steel B
Stress: 130MPa
Rupture Time: 1424h

Steel N
Stress: 120MPa
Rupture Time: 629h

0.5μm

Fig.8 TEM structures of test steels creep-ruptured at 650℃

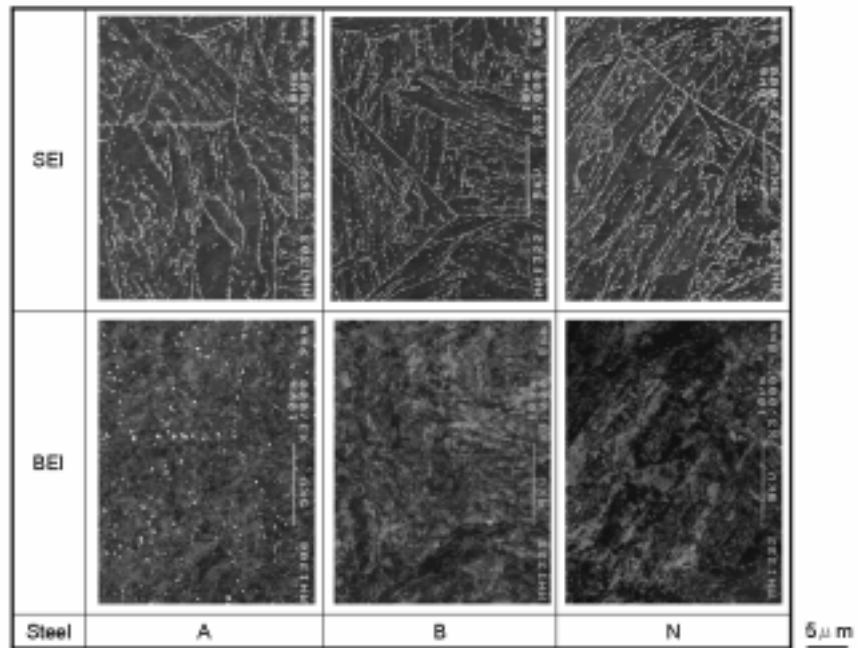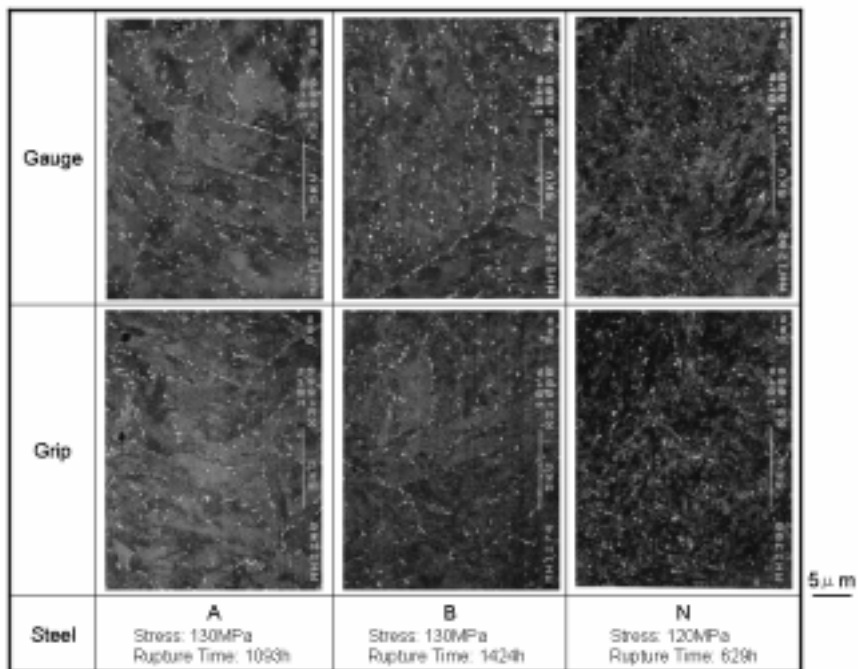Fig.9 FE-SEM structures of test steels as-manufactured

Fig.10 FE-SEM BEI structures of test steels creep-ruptured at 650℃

MX under the as-manufactured conditions (normalized, tempered and annealed). In addition to these two precipitates, Laves phase was heavily generated in steel A, but hardly at all in steels B and N. It is also suggested that Laves phase appears in the all steels due to heating during the creep test, but without any effect on creep stress. The M₂X precipitation predicted by the kinetic

calculation was not observed in the experimental specimens in the present work. These results obtained from the actually melted steels differ from the phase prediction based on the thermodynamic and kinetic models mentioned previously.

Discussion

The predictions of the properties of steels designed using neural networks and phase stability calculations were tested experimentally. The major differences between predictions and experimental results were (1) creep rupture strength, and (2) precipitation of Laves phase and M_2X. The measured creep strength of the experimental specimens whose chemical compositions and heat treatment were nearly the same as predicted excepting silicon, nickel, copper and aluminum for steels A and B, and in addition to these cobalt for Steel B, was two fifths of the predicted values, but lay at the upper bound of the strongest existing steel (Grade 92). This was well reproduced by the predicted steel, steel N (10CrMoW), particularly at the temperatures of 600°C and 650°C. In comparison with commercial steel grades, the predicted steels A and B are approximately 5%, 30% and 40% stronger than Grades 92, 122 and 91 (7) respectively at 600°C and 100,000 h based on data with maximum testing duration of 23.500 h. As indicated above, some alloying elements were input as 0%, despite the fact that actual melting cannot achieve these ideal inputs. The roles of the 0% element are not certain in the designed steel, nor is the effect of the lean elements in the melted steels on creep strength reduction. Also, there exists no data on 0% silicon, nickel, copper and aluminum alloyed steels. As shown in Figure 4, elevated tensile strengths at 600°C and 650°C for each of the steels actually melted are at nearly the same level, but the creep rupture strengths of steels A and B are predicted as being extremely high against tensile strength. If the steel N exhibits a reasonable balance of tensile strength and creep strength, steels A and B would have the twice of tensile strength measured or 700 MPa at 600°C and 600 MPa at 650°C, which would be impractical. However, if an unbalanced relationship between tensile strength and creep strength could be accepted, the creep strength mechanism of steels A and B should be expected to differ from that of steel N. Nevertheless, the creep deformation mechanism and strengthening mechanism (precipitation strengthening) were confirmed to be the same in the previous section. It is considered that the lack of data on chemistry effects (particularly 0% elements) causes the prediction of mutation of creep rupture strength if there is no discontinuity in the effect of concentration of elements on the creep strength.

Precipitates observed in the test steels are nearly the same as in existing high strength ferritic steels, such as Grades 91, 92 and 122, excepting Laves phase precipitation. The Laves phase in general is not observed in steels normalized and tempered at temperatures above 730°C, typically 760°C and above, and generally applied as boiler steels. However, steel A showed considerable Laves phase after annealing at 740°C, and no Laves phase was also observed in steels B and N. Annealing followed by air cooling is somewhat effective in Laves phase generation, and steel A contains a larger quantity of molybdenum compared with steels B and N, and large amount of tungsten. Phase stability calculations at the equilibrium state suggested Laves phase formation, and the kinetic model predicted Laves phase after long term heating at

650°C for steel N, but not for steels A and B. Meanwhile, it was predicted that M_2X would form in all steels due to the short time of heating. In fact, the test steels formed $M_{23}C_6$, MX and Laves phase before and after the creep test. It is also not certain whether the 0% elements affect precipitation behavior, or why M_2X (Cr_2N based precipitation) occurs in the kinetic calculation, as opposed to MX in the designed and actually melted steels.

Conclusions

A combination of mechanical property models based on neural networks together with phase stability calculations relying on thermodynamics has proposed new ferritic steels for power applications, and these predictions were tested experimentally. The results obtained from this work are as follows:

(1) The major differences between the predictions and the experimental results were regarding creep rupture strength and the precipitation of Laves phase and M_2X.

(2) The creep strength of the experimental specimens was two fifths of the predictions, but lay at the upper bound of the strongest existing steel (Grade 92), and this was well reproduced by the predicted steel, steel N (10CrMoW), particularly at the temperatures of 600°C and 650°C. In comparison with commercial steel grades, the predicted steels A and B are approximately 5%, 30% and 40% stronger than Grades 92, 122 and 91 respectively at 600°C and 100,000 h.

(3) The experimental specimens formed precipitates consisting of $M_{23}C_6$, MX and Laves phase before and after the creep test despite the prediction of precipitates in the designed steels of $M_{23}C_6$ and Laves phase at the equilibrium state, and of $M_{23}C_6$ and M_2X on the kinetic time scales.

References

(1) F. Masuyama, "History of Power Plants and Progress in Heat Resistant Steels", ISIJ International, Vol. 41, No. 6, (2001), pp. 612 – 625.

(2) F. Masuyama, "Advanced Power Plant Developments and Material Experiences in Japan", J. Lecomte-Beckers, et al. (eds), Materials for Advanced Power Engineering, Part I, Forschungszentrum Juerich GmbH, Germany, (2006), pp. 175 – 187.

(3) H. K. D. H. Bhadeshia, "Neural Networks in Materials Science", ISIJ International, Vol. 39, No. 10, (1999), pp. 966 – 979.

(4) F. Brun, T. Yoshida, J. D. Robson, V. Narayan, H. K. D. H. Bhadeshia and J. C. Mackay, "Theoretical Design of Ferritic Creep Resistant Steels using Neural Network, Kinetic, and Thermodynamic Model", Materials Science and Technology, Vol. 15, (1999), pp. 547 – 554.

(5) H. Mimura, M. Ohgami, H. Naoi and T. Fujita, "Properties of 9Cr-1.8W Steel with High Creep Strength for USC Boiler Piping and Tubing Applications", D. Coutssouradis, et al. (eds.), Materials for Advanced Power Engineering 1994, Part I, Kluwer Academic Publishers, Netherlands, (1994), pp. 361 – 372.

(6) F. Masuyama and N. Komai, "Evaluation of Long-term Creep Rupture Strength of Tungsten-strengthened Advanced 9-12%Cr Steels", Key Engineering Materials, Vol. 171-174, (2000), pp. 179 – 188.

(7) K. Kimura, "Review of Allowable Stress and New Guideline of Long-term Creep Strength Assessment for High Cr Ferritic Creep Resistant Steels", I. A. Shibli, et al. (eds.), Creep & Fracture in High Temperature Components -Design & Life Assessment Issues-, DEStech Publications, Pennsylvania, (2005), pp. 1009 – 1022.